TEST CASE DOCUMENTATION
AND TESTING RESULTS

TEST CASE ID ICFD-VER-7.1

Conjugate forced convection

Tested with LS-DYNA® R7 Revision

Saturday 2nd February, 2013

LSTC
Livermore Software
Technology Corp.

Document Information	
Confidentiality	**external use**
Document Identifier	LSTC-QA-LS-DYNA-ICFD-VER-7.1-1
Author(s)	Iñaki Çaldichoury, Facundo Del Pin
Number of pages	22
Date created	Saturday 2nd February, 2013
Distribution	External

Disclaimer:

Contents

1 Introduction

1.1 Purpose of this Document

This document specifies the test case ICFD-VER-7.1. It provides general test case information like name and ID as well as information to the confidentiality, status, and classification of the test case.

A detailed description of the test case is given, the purpose of the test case is defined, and the tested features are named. Results and observations are stated and discussed. Testing results are provided in section 4.1 for the therein mentioned LS-DYNA® version and platforms.

2 Test Case Information

Test Case Summary	
Confidentiality	external use
Test Case Name	Conjugate forced convection: Longitudinally periodic regime
Test Case ID	ICFD-VER-7.1
Test Case Status	Under consideration
Test Case Classification	Verification
Metadata	THERMAL PROBLEM

Table 1: Test Case Summary

3 Test Case Specification

3.1 Test Case Purpose

This present test case aims at validating the Conjugate heat transfer solver both in 2D and 3D using the analytical solutions of conjugate heat transfer problems involving a parallel plane channel (2D case) or a cylindrical channel (3D case) with a longitudinally periodic regime for the temperature.

3.2 Test Case Description

3.2.1 Introduction

In [2] and [3] the analytical solution of the conjugate heat transfer problem in a parallel-plane channel has been studied for two kinds of boundary condition prescribed on the exterior channel of the solid. The boundary condition is either defined by a temperature imposition which varies longitudinally with sinusoidal law ($T = T_0 + \Delta T sin(\beta z)$) or by a prescribed heat flux ($q = q_0(1 + \lambda sin(\beta z))$). In [1], the problem has been extended to the axi-symmetric cylindrical channel case with a periodic prescribed temperature boundary condition. In all cases, the flow is considered laminar and fully hydrodynamically and thermally developed. Numerous industrial applications meet such conditions and are often encountered in nuclear reactor cooling designs, heat exchangers for Stirling-cycle machines or internally finned ducts [2]. Figure (1) offers a sketch of the complete fluid-solid conjugate heat transfer problem.

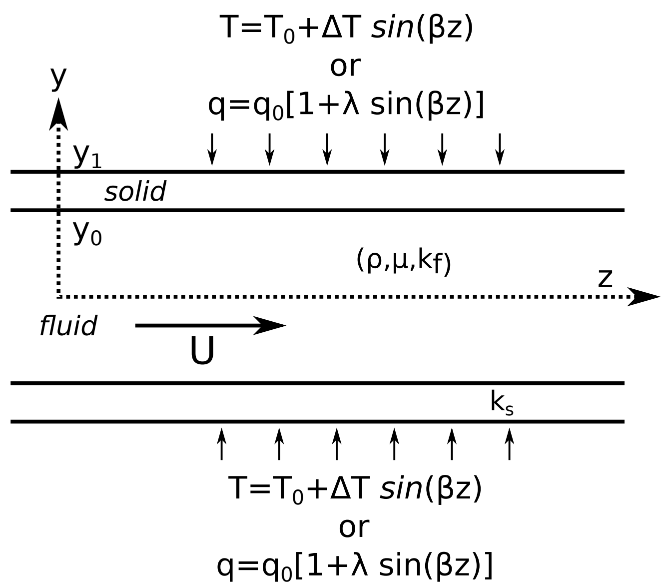

Figure 1: Sketch of the longitudinal section of the channel

3.2.2 Dimensionless Parameters

As in most fluid mechanics problems, it is often more convenient to work in dimensionless quantities :

$$\begin{aligned}
\eta &= \frac{y}{y_0} && (1)\\
\epsilon &= \frac{z}{z_0} && (2)\\
\sigma &= \frac{y_1}{y_0} && (3)\\
\theta_{TBL} &= \frac{T - T_0}{\Delta T} && (4)\\
\theta_{HFBL} &= k_f \frac{T - T_0}{q_0 y_0} && (5)\\
\gamma &= \frac{k_s}{k_f} && (6)\\
B &= Pe\beta y_0 && (7)\\
u &= \frac{U}{U_0} && (8)
\end{aligned}$$

with y_0 the half height of the internal channel wall, y_1 the half height of the exterior channel wall, z the axial coordinate of the channel, θ_{TBL} and θ_{HFBL} the adimensional temperature in the cases where the temperature or the heat flux are imposed as boundary condition, T the temperature (T_0, ΔT, q_0 and λv are input parameters that can be determined by the boundary condition imposed on the solid exterior channel wall), k_s and k_f the solid and fluid thermal conductivities respectfully, β the angular frequency, U and U_0 the longitudinal component of the fluid velocity and its mean value, and finally Pe the Peclet number.

The Peclet number is a dimensionless number relevant in the study of transport phenomena in fluid flows. It is defined as the rate of advection to the rate of diffusion of a given physical quantity which in the context of heat transports makes it equivalent to the product of the Prandtl and the Reynolds number :

$$Pe = Pr \times Re = \frac{U_0 y_0}{\alpha_f} \tag{9}$$

where α_f is the fluid thermal diffusivity equal to :

$$\alpha = \frac{k}{\rho c_p} \tag{10}$$

where ρ is the fluid's density and c_p is the fluid's heat capacity.

3.2.3 The analytical solution - 2D Temperature boundary condition

The temperature distribution has been obtained analytically in [2] by expressing the energy balance equation as a complex-valued hypergeometric confluent equation. The temperature profile (θ_{TBL}, simply given as θ here) can be written as :

$$\theta(\eta,\epsilon) = \theta_0(\eta) + \theta_1(\eta) sin(\frac{B\epsilon}{Pe}) + \theta_2 cos(\frac{B\epsilon}{Pe}) \tag{11}$$

where it has been shown in [2] that $\theta_0 = 0$ and θ_1, θ_2 can be expressed as the real and imaginary parts of the complex valued function $\psi(\eta)$:

$$\psi(\eta) = \begin{cases} C_1 e^{\frac{H\eta^2}{4}} {}_1F_1(\frac{2+H}{8}; \frac{1}{2}; -\frac{H}{2}\eta^2) & \text{for } 0 \leqslant \eta \leqslant 1 \\ C_2 e^{\frac{\eta B}{Pe}} + C_3 e^{-\frac{\eta B}{Pe}} & \text{for } 1 \leqslant \eta \leqslant \sigma \end{cases}$$

where $H = (i-1)\sqrt{3B}$, ${}_1F_1$ is the confluent hypergeometric function and C_1,C_2,C_3 are complex constant calculated using the temperature boundary conditions and given in [2].

Figure (2) and Figure (3) offer a 3D view of the dimensionless temperature behavior function of η and ϵ in the fluid and in the fluid+solid domain. The boundary between the solid and the fluid can be clearly identified with a change in temperature slope. A comparison between the two figures shows how the conductivity of the channel wall affects the temperature distribution. As expected with a more conductive solid, the gradient of temperature in the wall is less important. In cases where the wall conductivity is very high compared to the fluid conductivity, one can neglect the transverse temperature gradient and directly impose the solid temperature boundary condition on the fluid (CFD only analysis).

3.2.4 The analytical solution - 2D Heat flux boundary condition

The temperature distribution has been obtained analytically in [3] by expressing the energy balance equation as a complex-valued hypergeometric confluent equation. The temperature profile (θ_{HFBL}, simply given as θ here) is defined up to an arbitrary additive constant :

$$\theta(\eta,\epsilon) = \frac{A\epsilon}{Pe} + \theta_0(\eta) + \theta_1(\eta) sin(\frac{B\epsilon}{Pe}) + \theta_2 cos(\frac{B\epsilon}{Pe}) \tag{12}$$

where $A = 1$.

θ_0 can be expressed as ([3]) :

$$\theta_0(\eta) = \begin{cases} \frac{3}{4}\eta^2 - \frac{1}{8}\eta^4 & \text{for } 0 \leqslant \eta \leqslant 1 \\ \frac{\eta}{\gamma} + \frac{5}{8} - \frac{1}{\gamma} & \text{for } 1 \leqslant \eta \leqslant \sigma \end{cases}$$

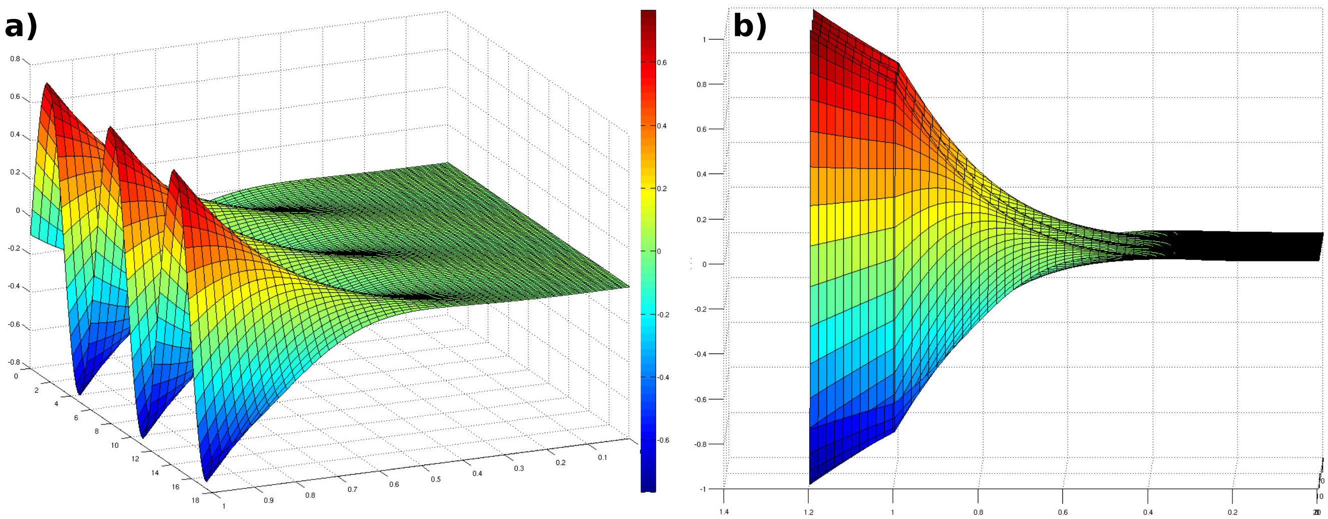

Figure 2: Analytical solution : dimensionless temperature distribution versus η and ϵ for $\sigma = 1.2$, $B = 100$, $Pe = 100$ and $\gamma = 3$, a) Fluid domain only, b) Fluid and Solid coupled domains.

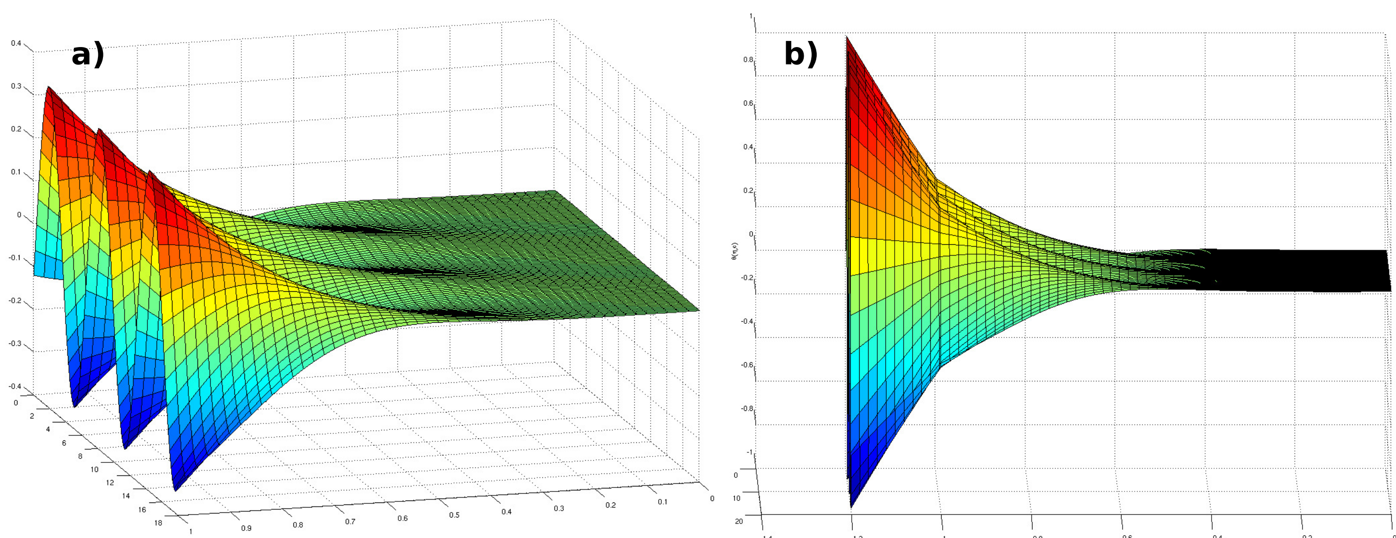

Figure 3: Analytical solution : dimensionless temperature distribution versus η and ϵ for $\sigma = 1.2$, $B = 100$, $Pe = 100$ and $\gamma = 0.5$, a) Fluid domain only, b) Fluid and Solid coupled domains.

And $\theta_0 = 0$ and θ_1, θ_2 can be expressed as the real and imaginary parts of the complex valued function $\psi(\eta)$:

$$\psi(\eta) = \begin{cases} C_1 e^{\frac{H\eta^2}{4}} {}_1F_1(\frac{2+H}{8}; \frac{1}{2}; -\frac{H}{2}\eta^2) & \text{for } 0 \leqslant \eta \leqslant 1 \\ C_2 e^{\frac{\eta B}{Pe}} + C_3 e^{-\frac{\eta B}{Pe}} & \text{for } 1 \leqslant \eta \leqslant \sigma \end{cases} \tag{13}$$

where $H = (i-1)\sqrt{3B}$, ${}_1F_1$ is the confluent hypergeometric function and C_1,C_2,C_3 are complex constant calculated using the heat flux boundary conditions and given in [3].

Figure (6) offers a 3D view of the dimensionless temperature behavior function of η and ϵ in the fluid+solid domain. When compared to Figure (3) and the imposed temperature boundary condition, it is interesting to note that the temperature behavior differs and seems to show a linear growth along the channel length. A higher λ value yields bigger amplitude differences.

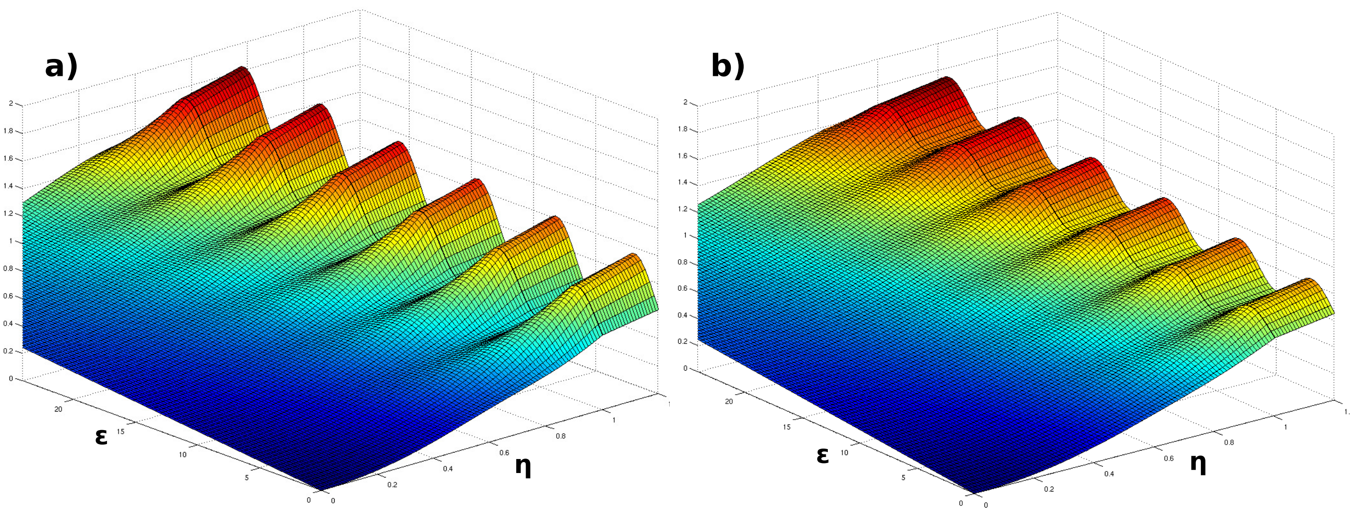

Figure 4: Analytical solution : dimensionless temperature distribution versus η and ϵ for $\sigma = 1.2$, $B = 100$, $Pe = 100$ and $\gamma = 3$, a) $\lambda = 1$, b) $\lambda = 0.5$.

3.2.5 The analytical solution - 3D Temperature boundary condition

For the 3D case, the 2D-axisymmetric analytical solution has been demonstrated by [1] for a periodic temperature boundary condition as :

$$\theta(\eta, \epsilon) = \theta_0(\eta) + \theta_1(\eta) sin(\frac{B\epsilon}{Pe}) + \theta_2 cos(\frac{B\epsilon}{Pe}) \tag{14}$$

where $\eta = \frac{r}{r_0}$ and r is the channel radius. It has been shown in [1] that $\theta_0 = 0$ and θ_1, θ_2 can be expressed as the real and imaginary parts of the complex valued function $\psi(\eta)$. $\psi(\eta)$ can be expressed in the fluid domain as the following power series :

$$\psi(\eta) = \begin{cases} C_1 \left(\Gamma(\frac{1-w}{2})\right)^{-1} \sqrt{2w}\, e^{-w\eta^2} \times \sum\limits_{n=0}^{\infty} \frac{\Gamma(n+\frac{1-w}{2})}{n!\,n!} (2w\eta^2)^n & \text{for } 0 \leqslant \eta \leqslant 1 \\ C_2 I(0, \frac{B}{Pe}\eta) + C_3 K(0, \frac{B}{Pe}\eta) & \text{for } 1 \leqslant \eta \leqslant \sigma \end{cases}$$

where Γ is the gamma function and I, K are the first and second type Bessel functions respectively. Figure (5) offers a 3D view of the dimensionless temperature behavior function of η and ϵ in the fluid+solid domain.

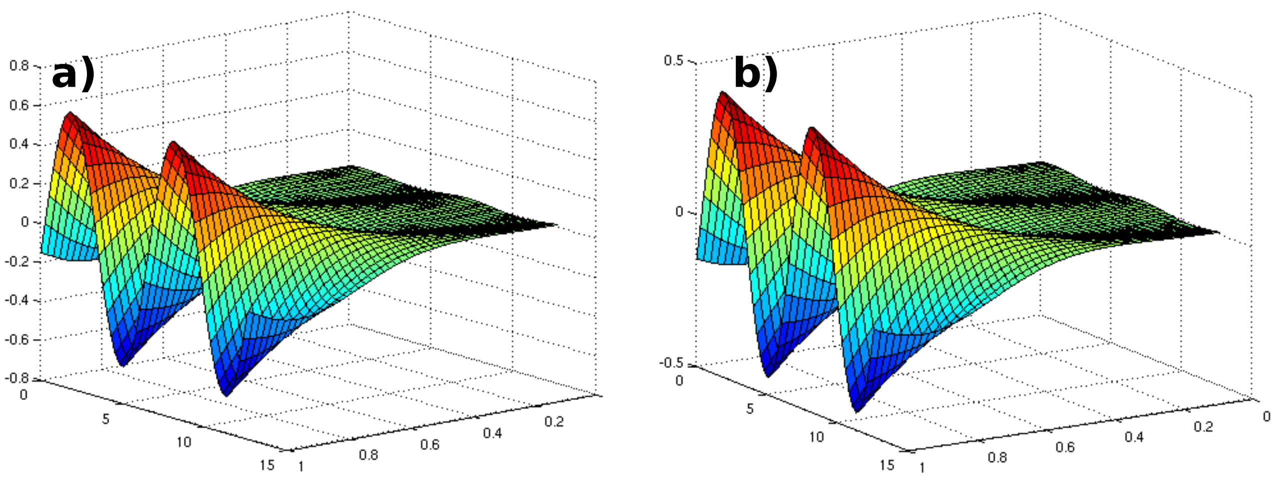

Figure 5: Analytical solution : dimensionless temperature distribution versus η and ϵ for $\gamma = 3$, $B = 100$, $Pe = 100$ and, a) $\sigma = 1.2$, b) $\sigma = 1.4$.

3.3 Model Description

Table (2), Table (3) and Table (4) offer some information on the model's chosen dimensions, mesh and parameters. For the sake of the analysis, Pe, B and γ and the solid thickness σ will be varied. The total length of the problem has been chosen so as to ensure a fully developed profile at the fluid-solid interface for the range of tested parameters. The 3D channel is half as long as the 2D channel in order to save some computational time but still long enough to ensure that a fully developed profile exists for all tested cases. Figure (6) offers a view of the mesh.

Model dimensions	
y_0	1
$2D\ channel\ Length$	120
$3D\ channel\ Length$	60

Table 2: Test Case Geometry Information

Model information	
Fluid Surface Element size	0.05
2D Fluid Volume Nodes	35 000
2D Fluid Volume Elements	68 000
3D Fluid Volume Nodes	350 000
3D Fluid Volume Elements	2 000 000
Number of elements through solid thickness	5
Anisotropic elements added to the boundary layer mesh	2

Table 3: Test Case Mesh Information

Model physical parameters	
Fluid Density	1
Viscosity	0.005
Inflow velocity ($= U_0$)	0.5
Reynolds number	100
Fluid thermal conductivity	1
Fluid thermal heat capacity	*variable*
T_0	80
ΔT	20
q_0	10
B	*variable*
γ	*variable*
λ	*variable*
σ	*variable*

Table 4: Test Case Parameters

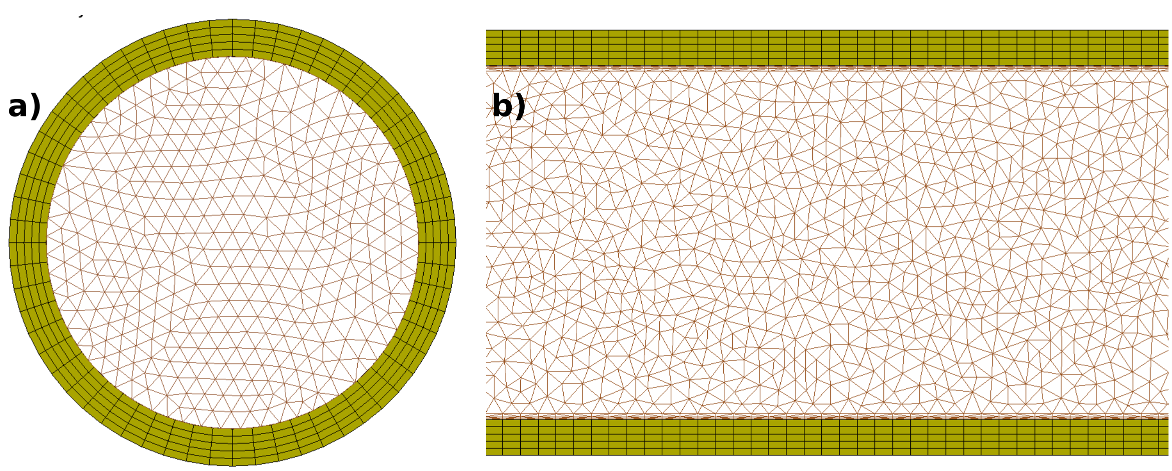

Figure 6: a) 3D surface mesh view, b) 2D mesh view

4 Test Case Results

4.1 Test Case observations

4.1.1 2D-Constant Temperature Boundary Condition case

The continuity of temperature at the interface is well insured by the numerical simulation as can be observed on Figure (7). Figure (8) offers a qualitative comparison between the analytical and the numerical temperature profiles at the solid-fluid interface. In Figure (9), the dimensionless temperature distribution at the solid-fluid interface is reported and a comparison is made with the analytical solution for $B = 100$, $\sigma = 1.2$, $\gamma = 3$ and for three different values of the Pe number. A higher Peclet number yields a smaller amplitude at the interface. This is consistent as a higher Peclet number value implies more temperature advection and on the other hand, an infinitely small Pecklet number would mean that the fluid has no influence on the solid temperature distribution. In Figure (10), the dimensionless temperature distribution at the solid-fluid interface is reported and a comparison is made with the analytical solution for $Pe = 100$, $\sigma = 1.2$, $\gamma = 3$ and for three different values of B. The figure shows that the period of the axial temperature distribution strongly differs in the three considered cases, while the oscillation amplitude does not display strong differences. Figure (11) shows again the dimensionless temperature distribution at the interface for three different values of γ. As expected, a higher γ value yields a temperature distribution closer to the boundary condition profile imposed at $\eta = \sigma$. Finally Figure (12) and Figure (13) show for two different sets of B and Pe the temperature profiles at different η along the channel. In both cases for all η values, the progressive alignment of the numerical solution with the analytical solution can be observed i.e the progressive establishment of the developed thermal profile. As a conclusion, all figures show an excellent agreement with the analytical solutions.

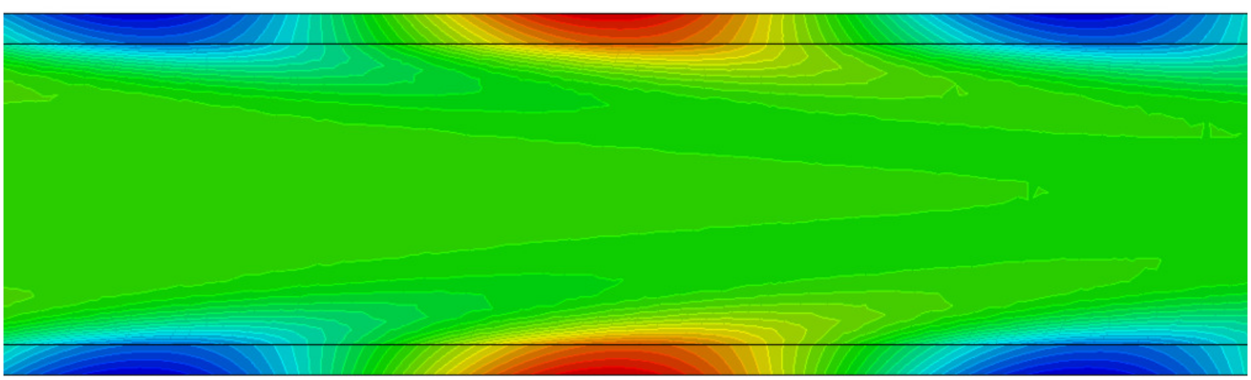

Figure 7: Numerical solution : temperature distribution in the fluid-solid domain for $\sigma = 1.2$, $\gamma = 3$, $Pe = 100$ and $B = 100$

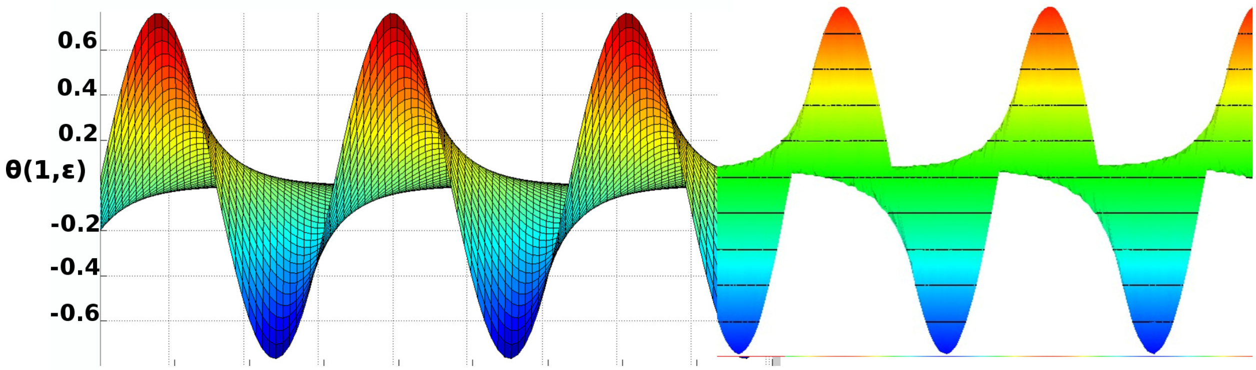

Figure 8: Dimensionless temperature : Qualitative comparison between the numerical and analytical results for the dimensionless temperature at $\eta = 1$ and for $\sigma = 1.2$, $\gamma = 3$, $Pe = 100$ and $B = 100$

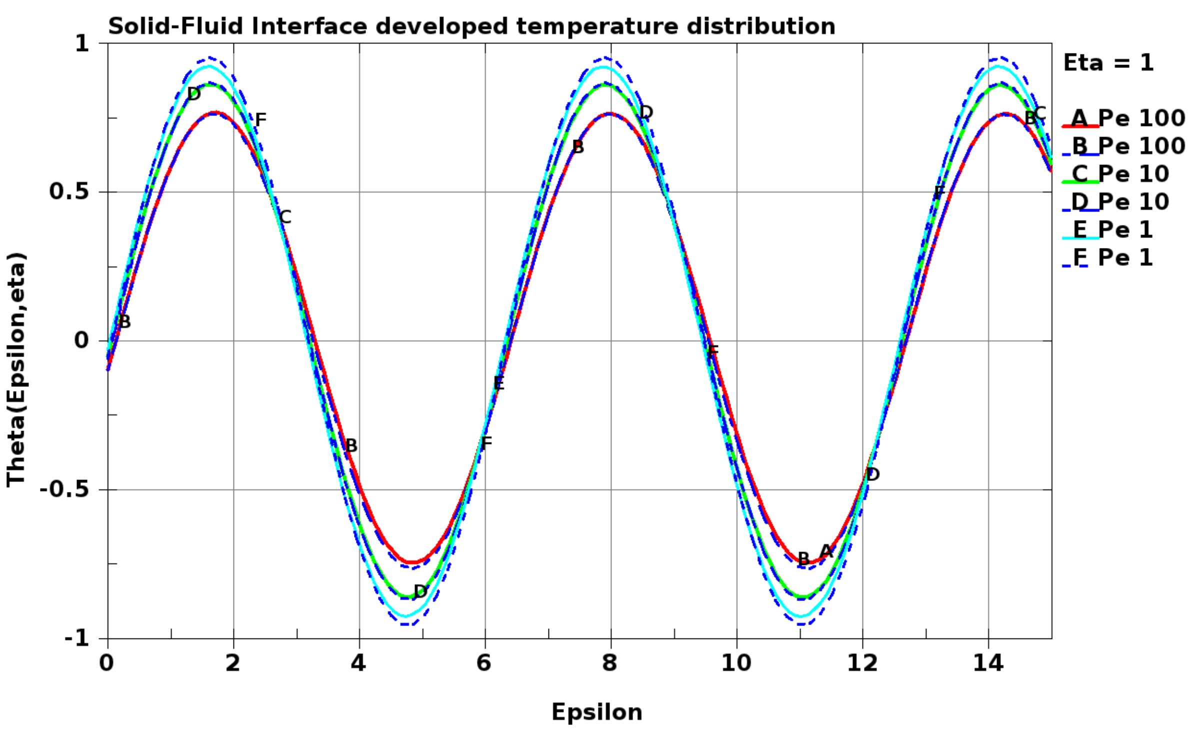

Figure 9: Dimensionless temperature distribution : comparison between the analytical solution (in Blue) and the numerical solution for $\eta = 1$, $\sigma = 1.2$, $\gamma = 3$, $B = 100$ and for three different values of the Peclet number in the hydrodynamically and thermally developed region.

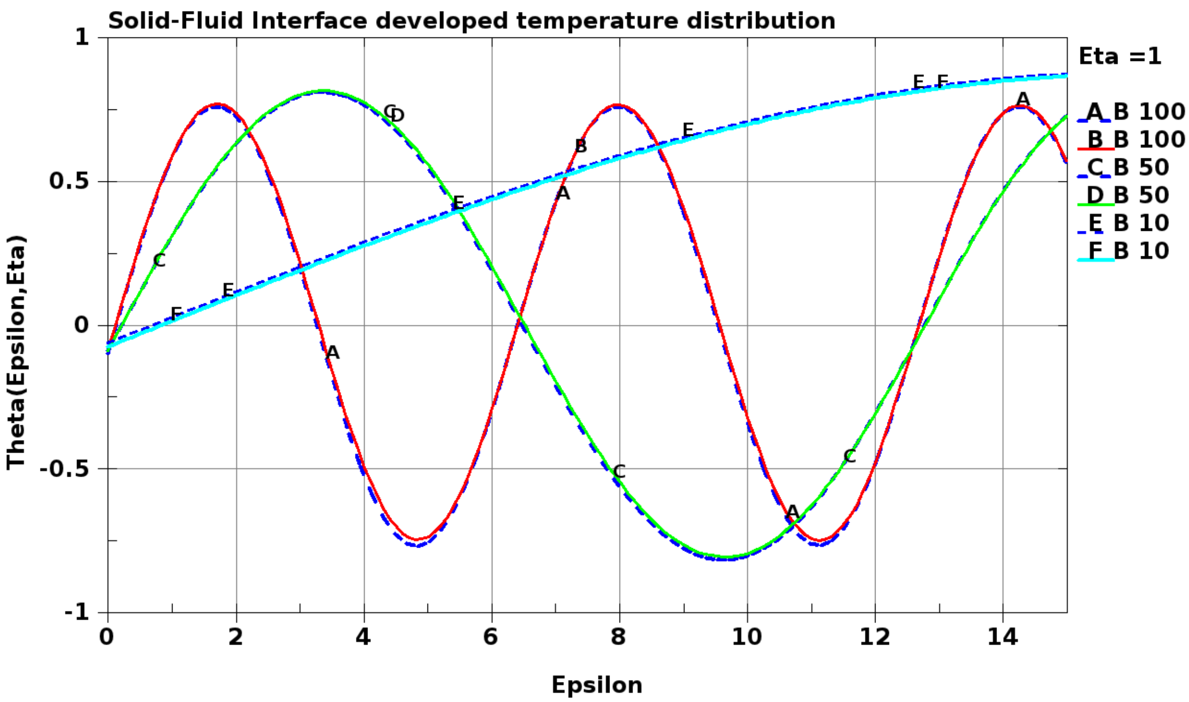

Figure 10: Dimensionless temperature distribution : comparison between the analytical solution (in Blue) and the numerical solution for $\eta = 1$, $\sigma = 1.2$, $\gamma = 3$, $Pe = 100$ and for three different values of the parameter B in the hydrodynamically and thermally developed region.

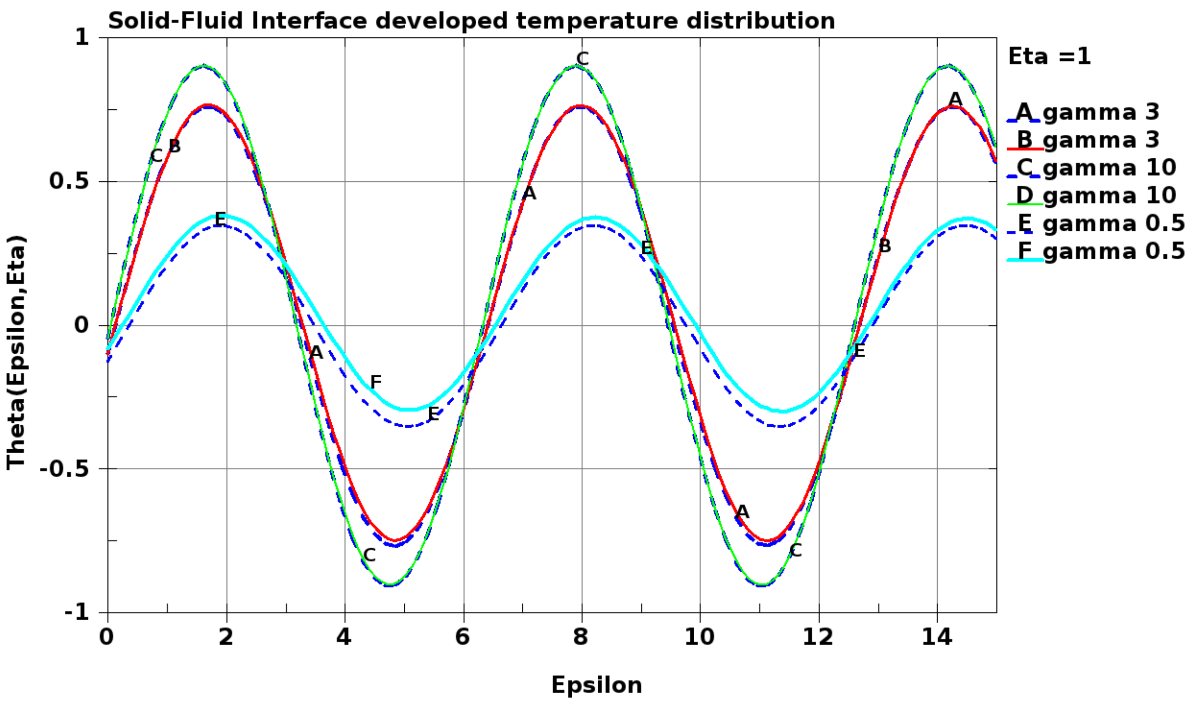

Figure 11: Dimensionless temperature distribution : comparison between the analytical solution (in Blue) and the numerical solution for $\eta = 1$, $\sigma = 1.2$, $B = 100$, $Pe = 100$ and for three different values of the parameter γ in the hydrodynamically and thermally developed region.

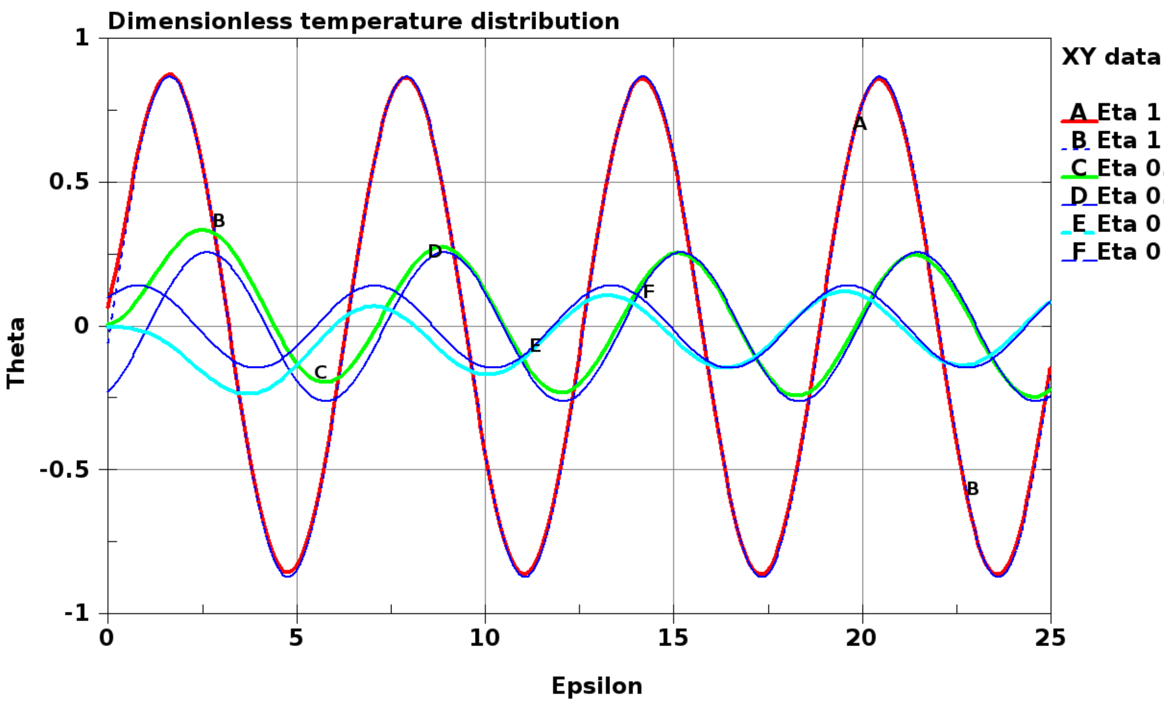

Figure 12: Dimensionless temperature distribution : comparison between the analytical solution (in Blue) and the numerical solution for $\gamma = 3$, $\sigma = 1.2$, $B = 10$, $Pe = 10$ and for three different values of the parameter η along the channel

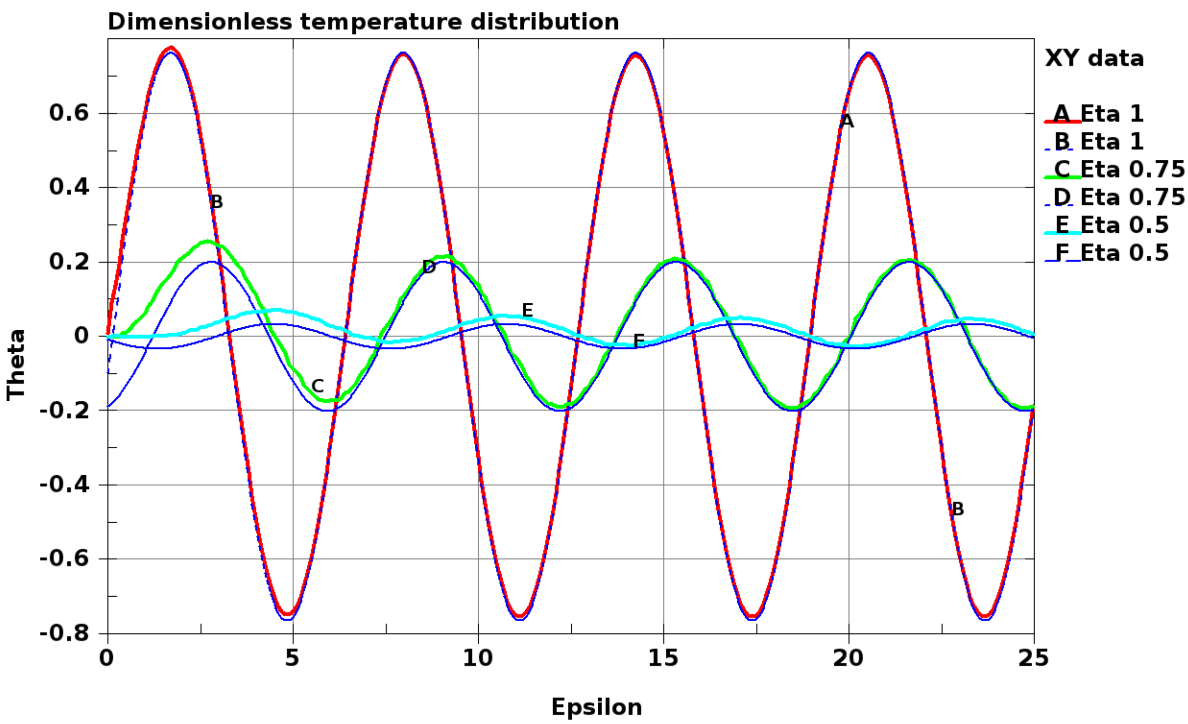

Figure 13: Dimensionless temperature distribution : comparison between the analytical solution (in Blue) and the numerical solution for $\gamma = 3$, $\sigma = 1.2$, $B = 100$, $Pe = 100$ and for three different values of the parameter η along the channel

4.1.2 2D-Constant Heat Flux Boundary Condition case

Figure (14) shows the dimensionless temperature evolution across the channel for different values of η. The linear growth observed for the analytical solution is perfectly captured and, as in the temperature boundary condition case, the distance required for the temperature profile to be fully developed can again be observed. Figure (15) shows the fully developed dimensionless temperature distribution for two values of the λ parameter. Again, good agreement with the analytical solution can be observed.

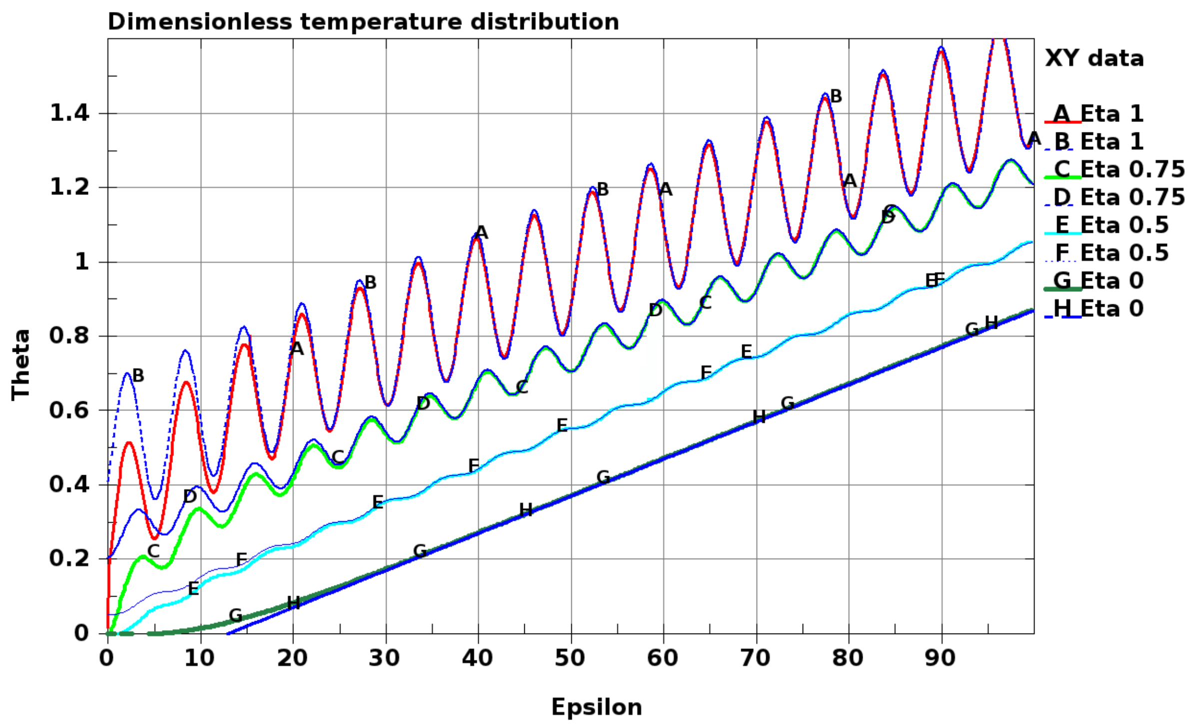

Figure 14: Dimensionless temperature distribution : comparison between the analytical solution (in Blue) and the numerical solution for $\gamma = 3$, $\sigma = 1.2$, $B = 100$, $Pe = 100$, $q_0 = 10$, $\lambda = 1$ and for four different values of the parameter η along the channel

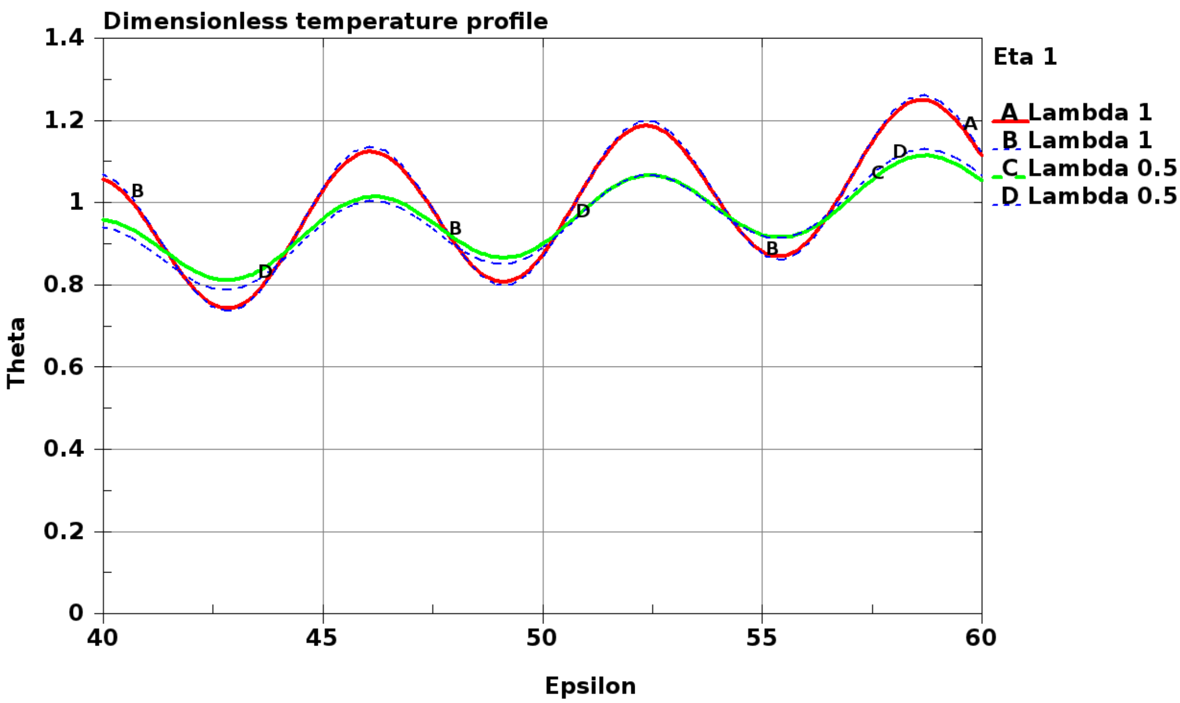

Figure 15: Dimensionless temperature distribution : comparison between the analytical solution (in Blue) and the numerical solution for $\sigma = 1.2$, $\gamma = 3$, $B = 100$, $Pe = 100$, $q_0 = 10$ at the solid fluid interface for two λ values

4.1.3 3D-Constant Temperature Boundary Condition case

As for the 2D case, the continuity of temperature between the solid and the fluid can be distinctly observed on Figure (16). Figure (17) further confirms the consistent behavior of the numerical solution. As expected, a higher Pe yields a higher temperature amplitude at the interface, a higher periodicity at the boundary impacts the frequency at the interface without impacting the amplitude, a lower thermal conductivity ratio gives a lower temperature at the interface as well as a bigger solid thickness which allows more temperature diffusion through the solid. The numerical solutions are in excellent agreement with the analytical solutions.

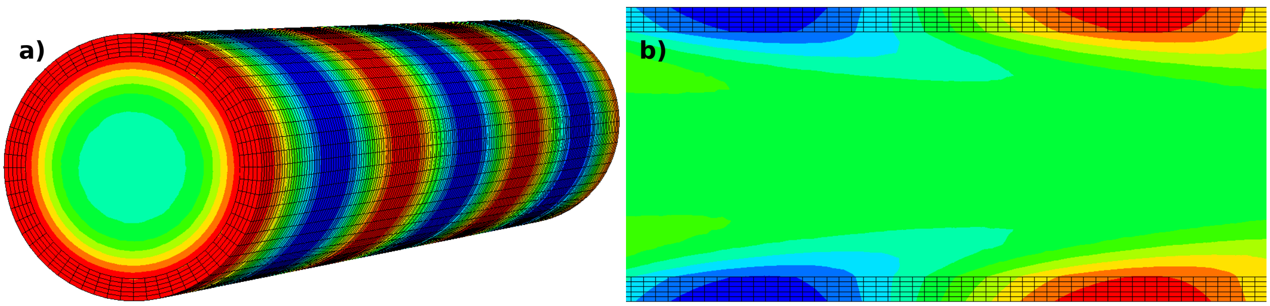

Figure 16: Numerical solution : temperature distribution in the fluid-solid domain for $\sigma = 1.2$, $\gamma = 3$, $Pe = 100$ and $B = 100$. a) 3D cut view b) Channel section cut.

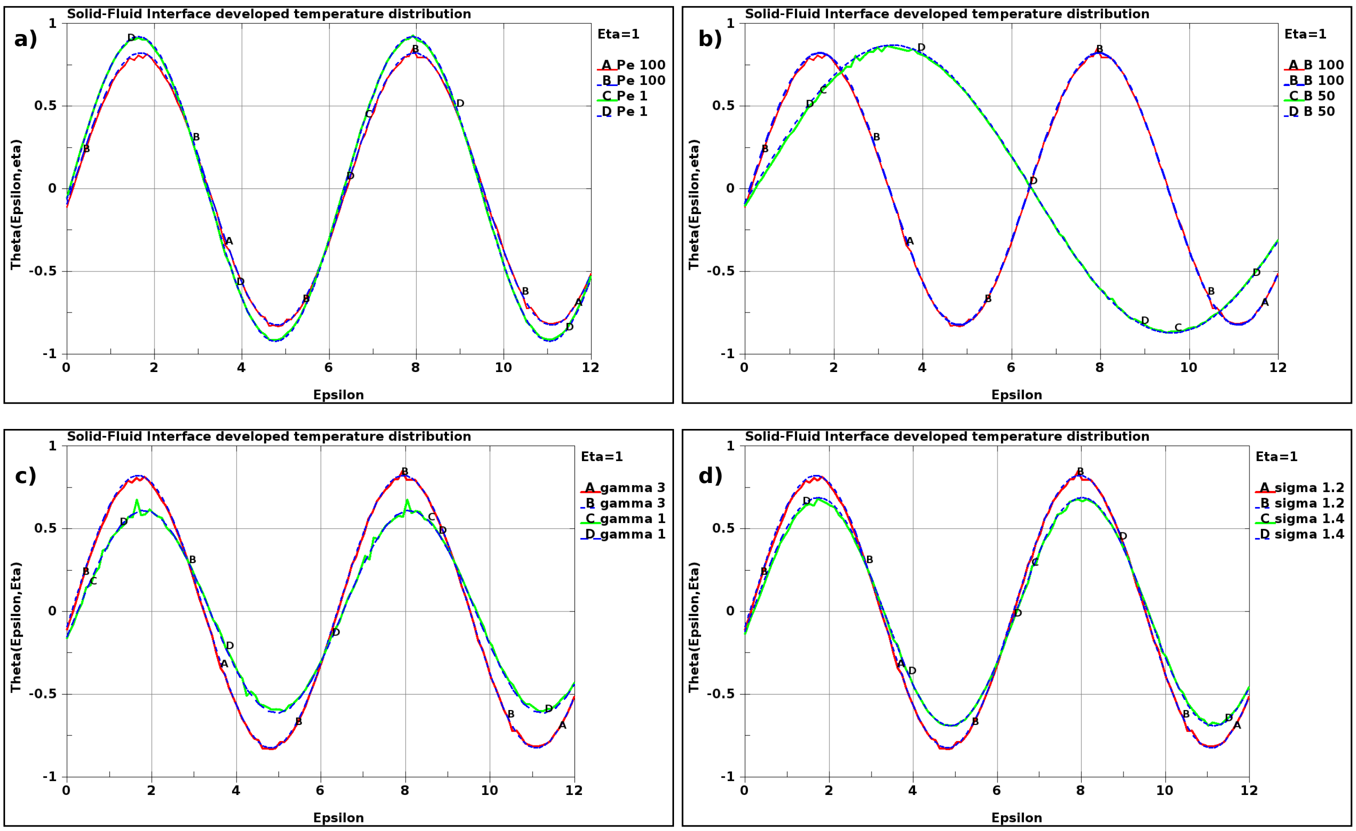

Figure 17: Dimensionless temperature distribution at the solid fluid interface : comparison between the analytical solution (in Blue) and the numerical solution for a) $\sigma = 1.2$, $\gamma = 3$, $B = 100$ and $Pe = variable$, b) $\sigma = 1.2$, $\gamma = 3$, $B = 50$ and $Pe = 100$, c) $\sigma = 1.2$, $\gamma = variable$, $B = 100$ and $Pe = 100$, d) $\sigma = variable$, $\gamma = 3$, $B = 100$ and $Pe = 100$

References

[1] M. R. Astaraki and N. G. Tabari, *Two-dimensional analytical solution of the laminar forced convection in a circular duct with periodic boundary condition*, Journal of Thermodynamics, 2012 (2012).

[2] A. Barletta, E. R. di Schio, G. Comini, and P. D'Agaro, *Conjugate forced convection heat transfer in a plane channel: Longitudinally periodic regime*, International Journal of Thermal Sciences, 47 (2008), pp. 43–51.

[3] ——, *Wall coupling effect in channel forced convection with streamwise periodic boundary heat flux variation*, International Journal of Thermal Sciences, 48 (2009), pp. 699–707.